Blood flow measurement using a highly filled carbon polymer sandwich sensor and an elasto-pseudo compressible vascular flow

M Mehdian, BSc, MSc, PhD, CEng, MIEE, MIEEE, FCybS
School of Engineering, University of Greenwich, London

H Rahnejat, BSc, MSc, PhD, DIC, CEng, MIMechE, FCybS
Department of Mechanical and Manufacturing Engineering, University of Bradford

Vascular grafts are widely employed in clinical practice and still pose significant problems of compatibility and longevity, particularly when the prosthesis is to replace arteries of small diameter. Once a graft has been implanted in the vascular tree, there is no easy way of assessing its interactions with the surrounding tissue. Doppler flow probes or some imaging techniques are commonly used to monitor flow velocity in vascular prostheses. It is, however, difficult to monitor a patient's recovery on a continuous basis. Continuous means of measurement can be quite invaluable. This paper presents a high-carbon filled polymer (HCFP) sensor that is developed for blood flow measurement in vascular grafts. Furthermore, a computational fluid dynamics model of incompressible blood flow in elastic blood vessels is presented.

Key words: blood flow analysis, polymeric sensor, pulsative pseudo-compressible flow, elastodynamics of vascular prosthesis

NOTATION

a	$[W/g(1/K + DC_1/Ee]^{-1/2}$
A	cross-sectional area of the graft
B_1	body force on an element of fluid
C_1	constant of longitudinal constraint
C_n	constant relating to the nth mode
D	diameter of graft
D_n	constant relating to the nth mode
e	thickness of the graft/blood vessel
E	Young's modulus of elasticity for the graft
g	gravitational acceleration
H	pressure head of fluid
K	bulk modulus of fluid
L	length of prosthesis
n	number of modes/eigenvalues
R	radius of graft/blood vessel
t	time
v	fluid velocity
W	weight of fluid element
x_1	direction of fluid flow
Z	height of fluid element
α	elevation of prosthesis to horizontal datum
δx_1	change in length of a fluid element
δR	change in radius of prosthesis/vessel
λ	eigenvalue
ν	Poisson's ratio
σ_1	longitudinal stress
σ_2	circumferential stress

1 INTRODUCTION

The growth in transplant surgery has meant a proportional increase in demand for post-operative monitoring. In a large number of such operations vascular grafts are employed. When the prosthesis replaces arteries of small diameter the continuous monitoring of a patient's condition becomes quite difficult to achieve. Grafts implanted in the vascular tree of the hepatic artery or the portal vein in liver transplant patients are usually 6–8 mm in diameter. Means of continuous monitoring of blood flow pressures are regarded as ideal. One such approach using a polymeric sensor based on polyvinylidene fluoride (PVF_2) has been highlighted by Dario *et al.* (1). Unfortunately, the piezoelectric properties of PVF_2 change during the process of sterilization. Furthermore, it is not possible to measure static pressures with the PVF_2 sensor. Miniature strain gauges in current use are also difficult to position on the graft.

High-carbon filled polymer is conductive and contains a high percentage of carbon. The resistance of the HCFP film decreases with an increase in contact pressure. The main advantages of using HCFP are its low cost, linearity within a good range of applied pressure, compliance for ease of mounting and conformity to sensing surfaces, non-toxicity and ease of sterilization.

In this paper the authors describe a sandwich structure of the HCFP-based flow measuring sensor and its characteristics. Experimental apparatus for the measurement of both static and dynamic flow measurements using the sensor and simulating blood flow in arteries are described. Results obtained with silicone grafts and a skin-type graft are presented. Furthermore, a numerical model of blood flow in arteries is developed and the corresponding results are presented. High-carbon filled polymer-based sensors have been developed and used as tactile devices in robotic applications by the authors (2, 3).

2 SENSOR STRUCTURE

High-carbon filled polymer is a conductive polymer. Its resistance decreases with an increase in pressure. At atmospheric pressure its film resistance is approximately 50 kΩ. The HCFP is sandwiched between a thin copper

The MS was received on 14 June 1994 and was accepted for publication on 22 April 1996.

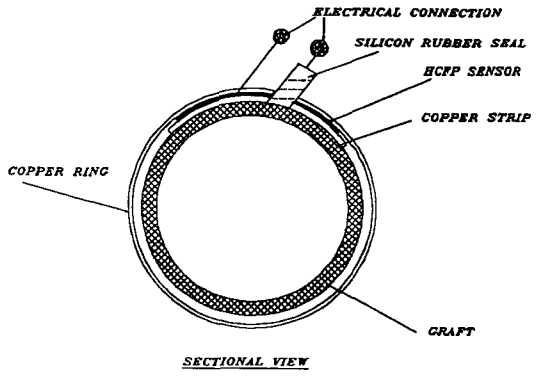

Fig. 1 High-carbon filled polymer sensor construction and mount

ring and a copper strip as shown diagramatically in Fig. 1. The electrical connections are soldered on to the copper ring and the inner copper strip. The wire connection from the inner copper strip is taken through silicone rubber insulation to prevent short circuiting. Figure 2 is a model mount of the sensor for demonstration purposes, giving an indication of sensor on graft assembly and the dimensions involved. A miniature clamp arrangement is used to open or close the sensing ring. This facilitates the ease of assembly/disassembly of the sensor. The sensor is non-invasive and does not interfere with the blood flow in the artery.

3 THE STATIC PRESSURE TEST RIG

A static pressure test rig is depicted in Fig. 3a and diagrammatically shown in Fig. 3b. It consists of a Perspex container with an internal diameter of 25 mm, an 'O' ring rubber seal, copper plates, a sphygmomanometer and the monitoring equipment. The HCFP is placed at the centre of the copper plates and can be regarded as a variable resistor. Since the sensor is fitted to the bottom end of the Perspex container the total pressure head is virtually normal to the sensor surface. An increase in pressure reduces the resistance of the sensor, thereby increasing its conductance and a higher voltage output is obtained. The following calibration procedure is adhered to:

1. The pressure is increased gradually from 0 mmHg to 200 mmHg using a sphygmomanometer.
2. The pressure is decreased from 200 mmHg to 0 mmHg in a gradual manner.
3. The sensor output is recorded at each pressure level.

4 THE BLOOD FLOW SIMULATION TEST RIG

The blood flow simulation test rig used for the monitoring of dynamic pressures is depicted in Fig. 4a and diagrammatically shown in Fig. 4b. It consists of a peristaltic pump, a solenoid valve, a sphygmomanometer, the HCFP-based sandwich sensor and the monitoring equipment. The sensor is fitted on the outer surface of the graft. Different pump operating frequencies, flowrates and pressures are used to determine the sensor characteristics with different types of grafts. The nature of the sensor output signal is pulsative. Thus, a Bessel filter is designed and employed to filter out the unwanted harmonics that occur above the frequency of 20 Hz. The following experimental procedure is adopted:

1. The pressure is gradually increased from 0 mmHg to 200 mmHg, using the sphygmomanometer.
2. The pressure is decreased gradually from 200 mmHg to 0 mmHg.
3. The sensor output in all cases is recorded and plotted against the rig pressure.

5 EXPERIMENTAL RESULTS

The results obtained using the static pressure rig are shown in Fig. 5. It can be observed that the sensor response is quite linear for the range of pressures of interest both in the loading and in the unloading cycles. Furthermore, the results in both parts of the cycle are quite close and repetitive tests have shown remarkable repeatability.

The results of real-time dynamic pressure monitoring using the blood flow simulation rig were obtained for various pump speeds and frequencies using either silicone tubing as a graft or a skin-type graft. The blood pumping frequencies for healthy persons in normal con-

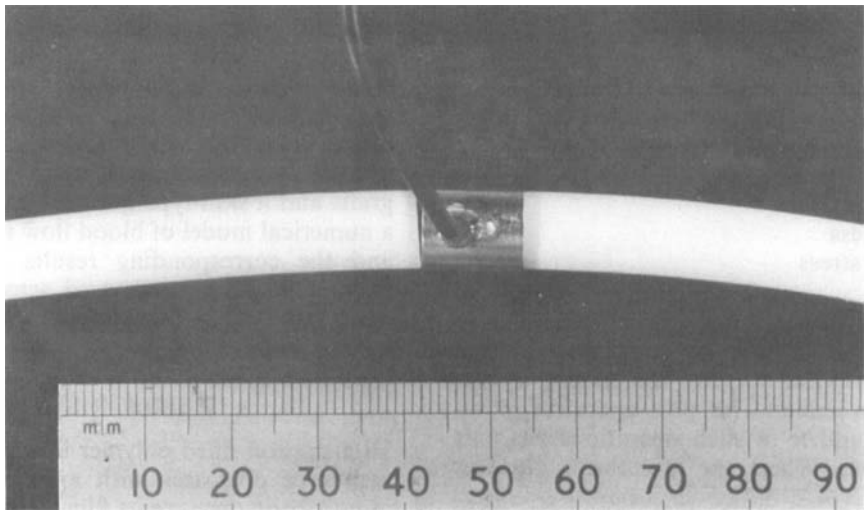

Fig. 2 A model mount of the sensor on a graft

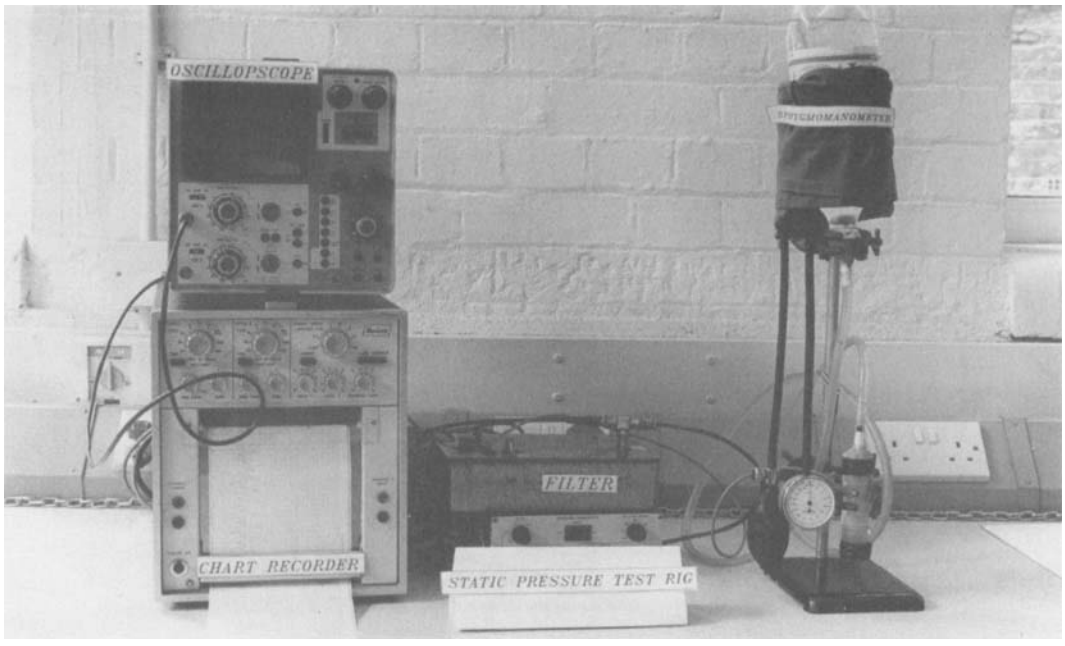

(a)

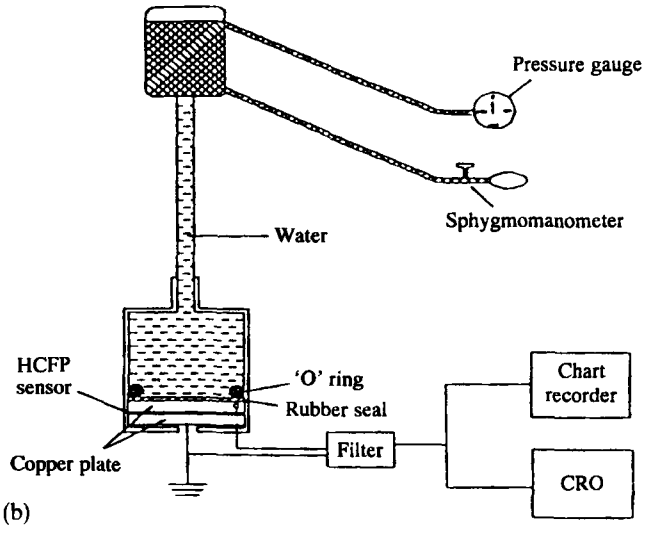

(b)

Fig. 3 The static pressure test rig

ditions lie between 0.63 and 2.0 Hz and the systolic pressure is slightly above 100 mmHg. The pump, however, runs at a flowrate of 2.53–4.00 cm^3/s and a speed of 50–100 r/min. The actual flowrate in a healthy person is approximately 8 cm^3/s. Nevertheless, the flow in both cases is laminar, having a Reynolds number between 690 and 2000 with a 6.4 mm diameter graft. Some of the results obtained with a silicone graft are shown in Fig. 6. These show a scatter and incorporate an unacceptable degree of non-linearity. It is concluded that the use of silicone-type grafts is not suitable in conjunction with this sensor. This is mainly due to the excessive thickness of the silicone tubing. An attempt was made to employ an actual vascular graft. However, due to its porosity and use of water as the simulating medium leakage resulted after several trials and the tests with the vascular graft were abandoned. It should be noted that the pores of vascular grafts are covered by blood cells. Finally, a skin-type graft was employed, in this study a semi-permeable PTFE-type was used. Some of the results obtained with the skin-type graft are shown in Fig. 7a and b. These indicate satisfactory sensor performance.

Pressure changes in the body are in fact relatively slow. This means that an adequate sensor output frequency response would enable absolute pressure measurements to be carried out. It should, however, be noted that the frequency response of the sensor is not high enough to achieve this.

6 BLOOD FLOW DYNAMICS MODEL

In order to obtain a relationship between the blood flowrate/blood flow speed and the sensor output, it is necessary to develop a numerical model of blood flow dynamics. This is particularly so because in the blood flow simulation rig water is employed as the fluid medium. The alternative is to undertake some animal experimentation which is seen to be outside the scope of the engineering research effort. Animal experimentation with the piezoelectric PVF_2 is reported by Dario *et al.* (1). There are also a host of medical safety consider-

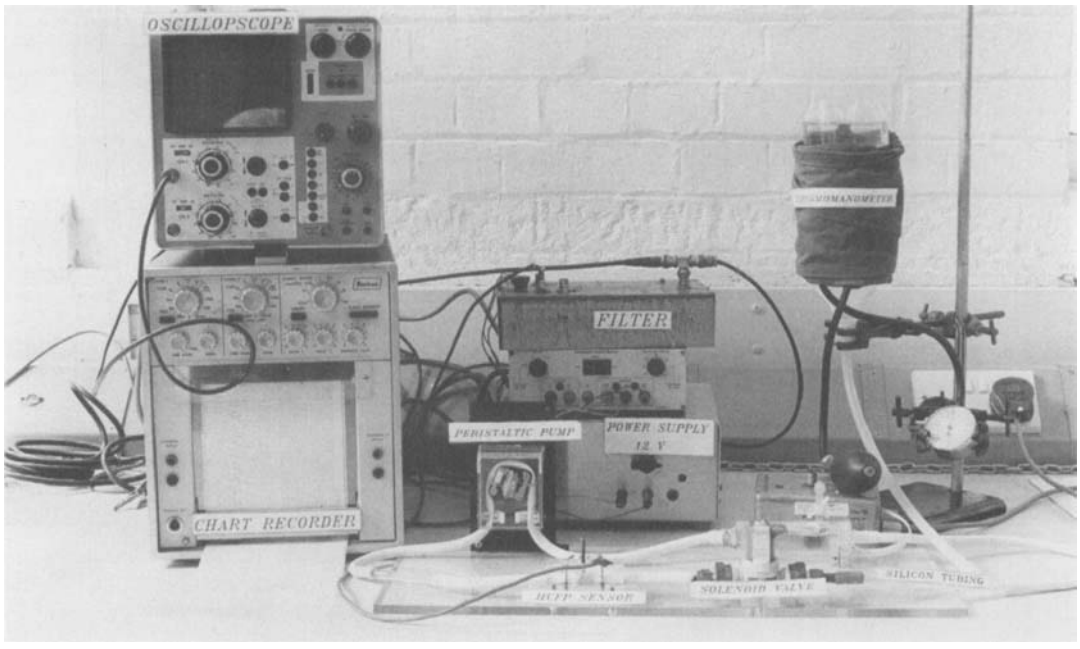

(a)

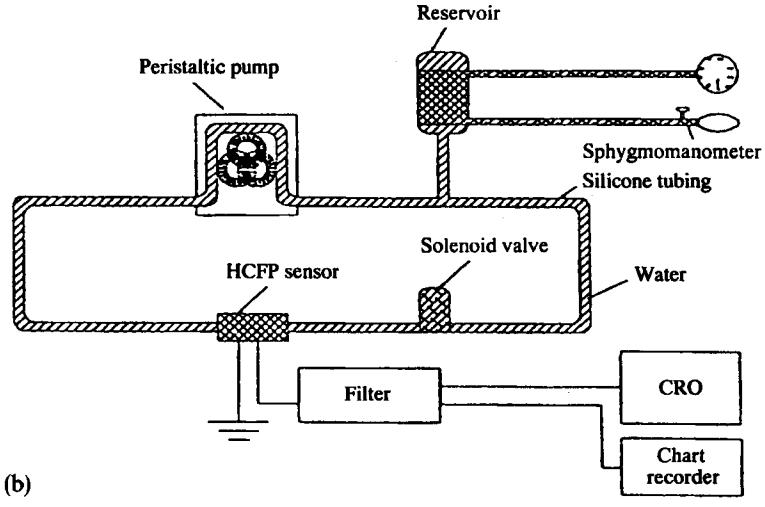

(b)

Fig. 4 The blood flow simulation test rig

ations in the use of vascular prostheses as highlighted by Montenson (4).

A computational fluid dynamics model of the blood flow simulation rig described above is formulated based on a general case of variable flow incorporating the elasticity of the blood vessel walls and the compressibility of the blood under the action of generated pressures. Blood volume changes occur as a result of the elasticity of the vessel walls as well as the changes in the magnitude of dynamic pressure. Therefore, a pseudo-compressible solution of blood flow is modelled. The conditions of flow continuity and dynamic equilibrium

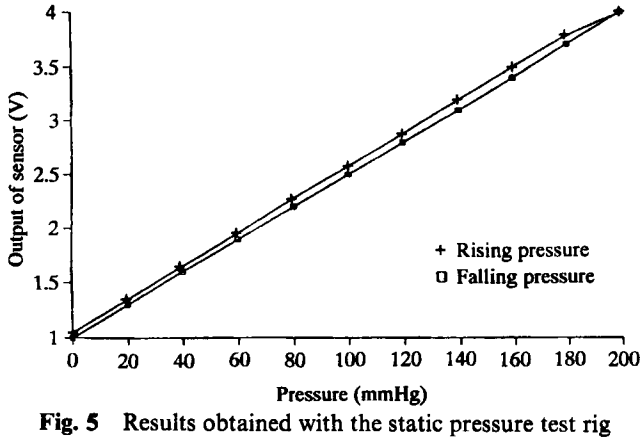

Fig. 5 Results obtained with the static pressure test rig

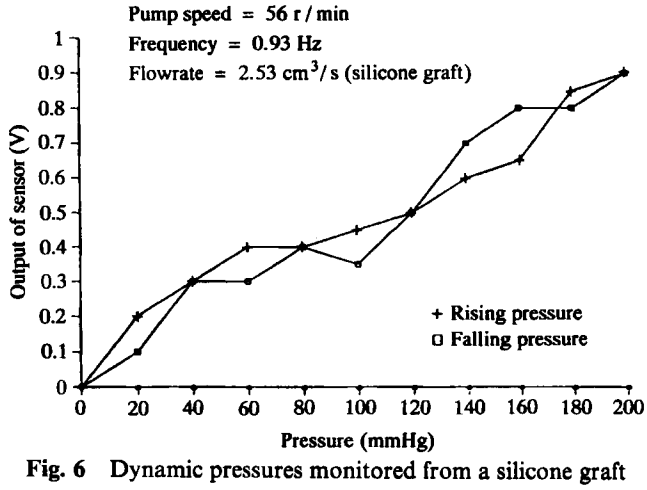

Fig. 6 Dynamic pressures monitored from a silicone graft

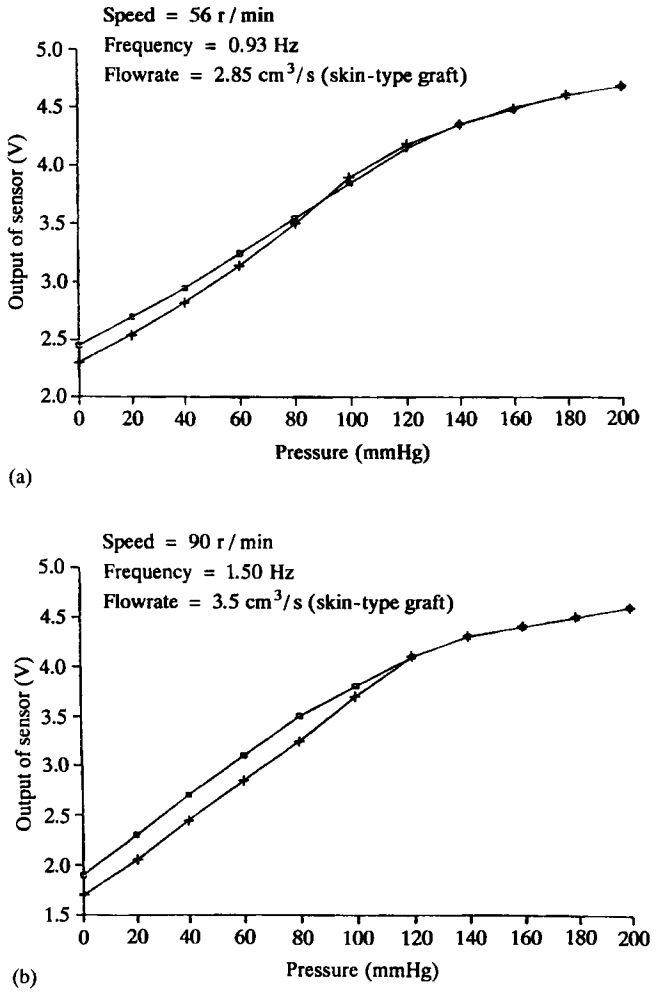

Fig. 7 Dynamic pressures monitored from a skin-type graft

of unbalanced forces acting on an element of blood are solved simultaneously to yield the fundamental flow equation.

The condition of dynamic equilibrium for an element of blood of length dx_1 is set up as shown in Fig. 8a. The gravitational (that is the body) force acting on the blood elemental mass of $WAdx_1/g$ is given by equation (1)

$$B_1 = W\left[A + \frac{1}{2}\left(\frac{\partial A}{\partial x_1}\right)\mathrm{d}x_1\right]\mathrm{d}x_1 \tag{1}$$

The unbalanced decelerating force acting along the axis of the blood vessel is

$$F = \left[A + \left(\frac{\partial A}{\partial x_1}\right)\mathrm{d}x_1\right]\left[H - Z + \left(\frac{\partial H}{\partial x_1} + \sin\alpha\right)\mathrm{d}x_1\right] - WA(H - Z) - W\left[A + \frac{1}{2}\left(\frac{\partial A}{\partial x_1}\right)\mathrm{d}x_1\right]\sin\alpha\,\mathrm{d}x_1 \tag{2}$$

where the positive direction of the force is taken opposite to the direction of normal flow.

Neglecting higher order terms and applying Newton's second law, where $a_1 = dv/dt$, then

$$\frac{\partial H}{\partial x_1} = -\left(\frac{\partial v}{\partial l} + v\frac{\partial v}{\partial x_1}\right) \tag{3}$$

where

$$\frac{\mathrm{d}v}{\mathrm{d}t} = \frac{\partial v}{\partial t} + v\frac{\partial v}{\partial x_1}$$

Equation (3) is the equilibrium equation for an element of blood.

A second equation relating H and v can be obtained by considering the condition of flow continuity. Referring to Fig. 8b, a very short interval of time $\mathrm{d}t$ has elapsed and an element of blood BC has moved to DF. There is a change in the length of the blood element in moving from BD to CF. This is primarily affected by two factors. Firstly, a change in pressure causes the blood vessel to expand or contract accordingly. The resulting change in the cross-sectional area produces a change in the length of the blood element in order to contain the same volume of blood. Secondly, because of the compressibility of blood, a change in pressure causes a corresponding change in the volume of blood within the blood element and as a consequence a further change in the length of the blood element results.

Neglecting the terms of the higher order

$$BD - CF = -\left(\frac{\partial v}{\partial x_1}\right)\mathrm{d}x_1\,\mathrm{d}t \tag{4}$$

The total change in the length of the blood element (that is $BD - CF$) can also be computed by considering the deformation of the blood vessel shell produced by changes in the longitudinal and circumferential stresses. Referring to Fig. 8c, the changes in radius and length are given by

$$\delta R = \left(\frac{2R + e}{2E}\right)[\delta\sigma_2 - v\,\delta\sigma_1] \tag{5}$$

$$\delta x_1 = \mathrm{d}x\sqrt{E(\delta\sigma_2 - v\,\delta\sigma_1)} \tag{6}$$

The volume enclosed by the newly stressed element is: $\pi(R + \delta R)^2(\delta x_1 + \mathrm{d}x_1)$, and the change in the length of the original element BC in Fig. 8b compatible with this change of volume is

$$\frac{\pi(R + \delta R)^2(\delta x_1 + \mathrm{d}x_1) - \pi R^2\,\mathrm{d}x_1}{\pi R^2}$$

After neglecting small terms, the total change in length of the element becomes

$$\delta x_1 + \frac{2\,\delta R}{R}\,\mathrm{d}x_1$$

The change in the longitudinal stress is dependent upon the ability of the blood vessel to move in the longitudinal direction. In general the total length extension produced by a pressure change of $W\,\mathrm{d}H$ is given by

$$\delta x_1 + \frac{2\,\delta R}{R}\,\mathrm{d}x_1 = \frac{C_1 WD\,\mathrm{d}H\,\mathrm{d}x_1}{Ee} \tag{7}$$

where C_1 is a constant depending on the condition of longitudinal constraint applied to the blood vessel element: $C_1 = 3/4 - v$ for a blood vessel restrained at its upper end and free to move in the longitudinal direction throughout its length and without expansion joints; $C_1 = 1 - v^2$ for a blood vessel which is restrained at its upper end and is constrained against

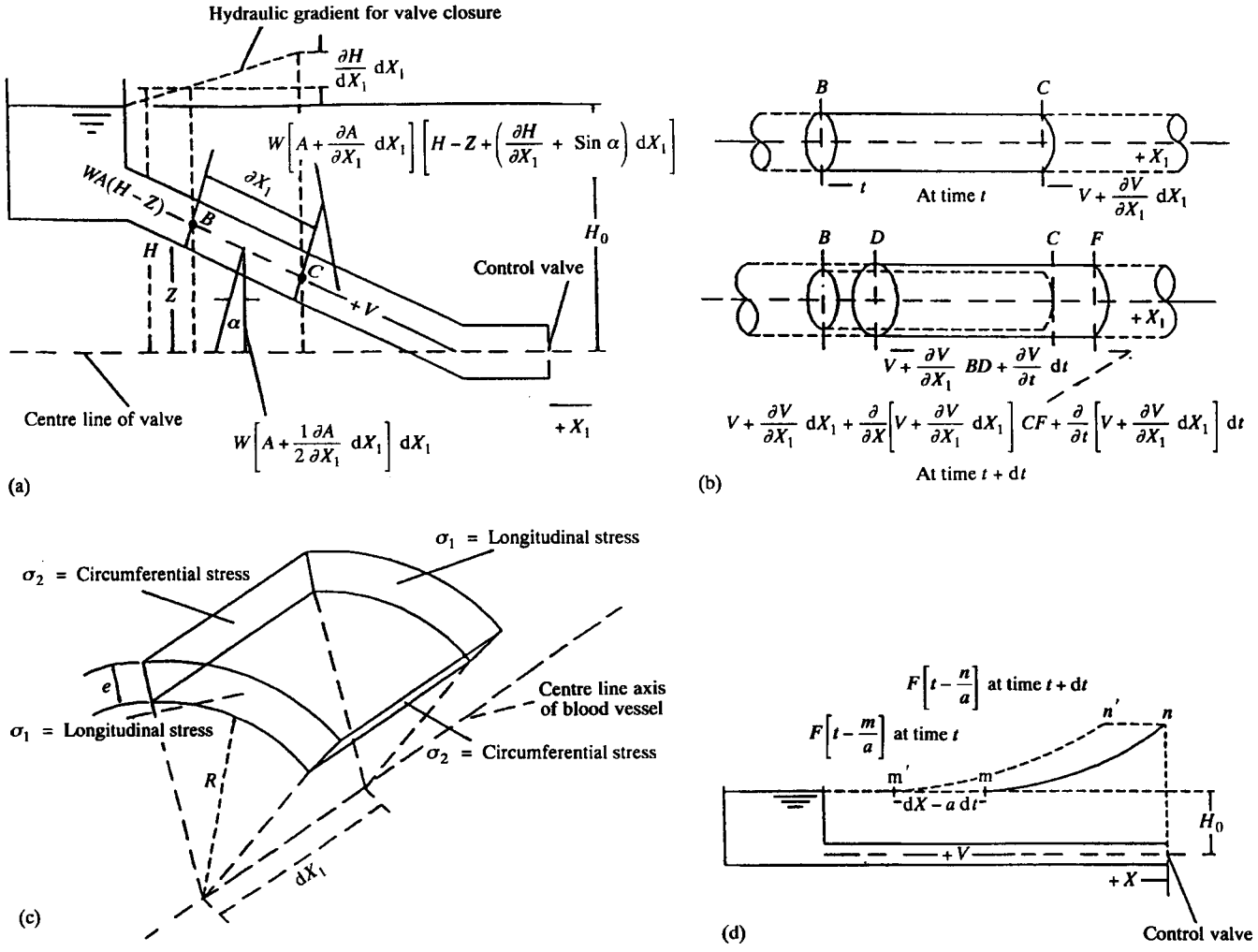

Fig. 8 The blood flow simulation model

any longitudinal movement throughout its length; and $C_1 = 1 - v/2$ for a blood vessel which has expansion joints between couples throughout its length.

The change in the volume of a blood element of length dx_1 due to blood compressibility under the action of a pressure change $W\ dH$ is $(W\pi R^2/K)\ dH\ dx_1$, which results in a corresponding blood element length change of $W\ dH\ dx_1/K$.

Therefore, taking into account both the blood compressibility and the blood vessel elasticity under pressure, the total change in the length of an element of blood is

$$\delta x_1 = W\left(\frac{1}{K} + \frac{DC_1}{Ee}\right) dH\ dx_1 \tag{8}$$

Since H is a function of x_1 and t, and $v = dx_1/dt$, it follows that the total change in the length of the blood element produced by a pressure change is given by equation (9) below

$$BD - CF = W\left(\frac{1}{K} + \frac{DC_1}{Ee}\right)\left(\frac{\partial H}{\partial t} + v\frac{\partial H}{\partial x_1}\right) dx_1\ dt \tag{9}$$

This equation can be equated with equation (4), yielding

$$\frac{\partial H}{\partial t} + v\frac{\partial H}{\partial x_1} = -\frac{a^2}{g}\frac{\partial v}{\partial x_1} \tag{10}$$

where

$$a = \left[\frac{W}{g}\left(\frac{1}{K} + \frac{DC_1}{Ee}\right)\right]^{-1/2} \tag{11}$$

Equation (10) is the continuity equation for the compressible blood flow in an elastic blood vessel (graft).

Equations (3) and (10) are the fundamental equations of blood flow. It can be shown (see Appendix 1) that the term $v\ \partial v/\partial x_1$ is small when compared with $\partial v/\partial t$ in equation (3), and the term $v\partial H/\partial x_1$ is small when compared with $\partial H/\partial t$ in equation (10). Therefore, the fundamental equations simplify to

$$\frac{\partial H}{\partial x_1} = -\frac{1}{g}\frac{\partial v}{\partial t} \tag{12}$$

$$\frac{\partial H}{\partial t} = -\frac{a^2}{g}\frac{\partial v}{\partial x_1} \tag{13}$$

7 SOLUTION AND PHYSICAL SIGNIFICANCE OF THE FUNDAMENTAL EQUATIONS

The general solution for the pair of the fundamental equations (12) and (13) is of the following form:

$$H - H_o = \phi(t + x\sqrt{a}) + \psi(t - x\sqrt{a}) \tag{14}$$

$$v - v_o = \frac{g}{a}\left[\phi(t + x_1\sqrt{a}) + \psi(t - x_1\sqrt{a})\right] \tag{15}$$

Both the functions ϕ and ψ are pressure heights which are measured in the same units as H. At a given instant of time they are both functions of x_1. After a small interval of time dt has elapsed, the arguments of these functions alter to

$$t + \mathrm{d}t - \frac{x_1 + \mathrm{d}x_1}{a}$$

and

$$t + \mathrm{d}t + \frac{x_1 + \mathrm{d}x_1}{a}$$

However, the magnitude of the functions remain unaltered provided that $x_1 = at + C_2$, where C_2 is a constant. Hence, the functions ϕ and ψ are pressure waves which move in the $+x_1$ and $-x_1$ directions respectively. They can be represented by certain curves such as mn shown in Fig. 8d for the function ψ for the simulation of the blood flow simulation rig described above.

The significance of solution equations (14) and (15) is now apparent. They imply that at any given time t at a point in the blood vessel with coordinate position x, the head rise is equal to the sum of the travelling pressure waves comprising ϕ and ψ. The waves are propagated in the opposite directions in the blood vessel with a constant velocity (for example for ψ from mn to m'n' in Fig. 8d). Furthermore, when a ϕ-wave passes a ψ-wave, neither wave is attenuated nor undergoes a change in shape. The numerical model for the solution of H and v consists of the solution of both wave equations ϕ and ψ as combination of sine and cosine functions with a number of modes, n. Thus, for example v as a function of a, n and t can be represented as (see Appendix 2)

$$v(x_1, n, t) = \frac{4L}{\pi^2} \sum_{n=1}^{\infty} \left(-(2n-1)^{-2} \sin\left[\frac{(2n-1)\pi at}{L}\right] \right) \times \left\{ (-1)^{n+1} \cos\left[\frac{(2n-1)\pi at}{L}\right] + \sin\left[\frac{(2n-1)\pi at}{L}\right] \right\} \quad (16)$$

A computer program is devised to calculate the values of H and v. The corresponding values of H and v for a given set of values of a, t and n are obtained and plotted, as shown in Fig. 9. As expected the flow speed increases linearly with an increase in the pressure head. Now the sensor output can be correlated to the flow velocity using the experimental results with the blood flow simulation rig (Fig. 7) and Fig. 9. The theoretical simulation results also provide the radial velocity profile at different times for various values of n and for a given cross-sectional position along the blood vessel or graft, as shown for example in Fig. 10. In this figure the profile corresponding to $t = 0$ depicts a maximum pulsatile situation. The subsequent velocity profiles indicate the situations after the maximum pulsation. The simulation can, therefore, aid in the positioning of the sensor on grafts in order to obtain a maximum signal output corresponding to the maximum pressure expected. The various times indicated in the figure are in ms, with $t = 0$ corresponding to the maximum flow-rate in the pulsatile flow condition. The use of Fig. 9 now becomes apparent, providing a corresponding radial pressure profile to the velocity profiles of Fig. 10, thus enabling the precise positioning of the sensor.

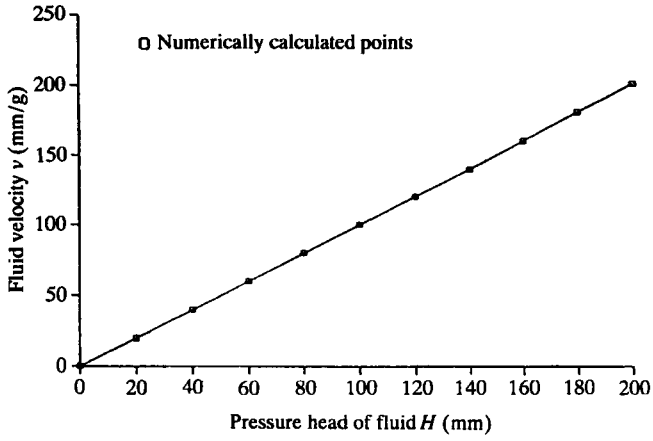

Fig. 9 Blood flow variation with the total head

8 CONCLUSIONS

The experimental results from the static pressure rig were found to be satisfactory. The sensor showed good linearity and repeatability. Care must be taken to

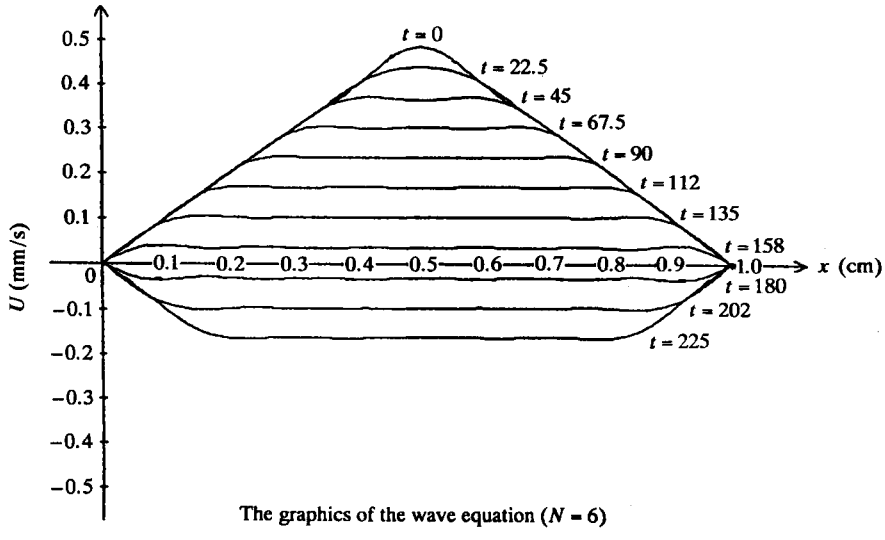

Fig. 10 Blood flow velocity profile as a function of time

prevent the copper strips from oxidization, since this would result in a change of conductivity. Copper strips should, therefore, be highly polished. Use of better materials for strips is perhaps more advisable, for example gold or platinum. Such choices would inevitably lead to expensive sandwich sensors. However, the cost would still amount to a fraction of that of Doppler probes.

Although the positioning of the sensor and its subsequent retrieval requires surgical procedures to be undertaken, the actual mounting of the sensor will not interfere with the blood flow in the prosthesis. In this context the prototype sensor may be considered as a non-invasive device.

The results from the blood simulation rig are not satisfactory with thick grafts such as silicone tubing but are acceptable with skin-type grafts. More work is needed with actual vascular grafts and prostheses. It is felt that trials with these should take place under medical supervision. In general the HCFP sensor has shown good potential for development for future practical applications.

REFERENCES

1 **Dario, P., Richardson, P. D.** and **Gall, P. M.** Monitoring of prosthetic graft using piezo-electric polymer sensors. *Trans. Am. Soc. Artif. Intern. Organs*, 1983, **XXIX**.

2 **Medhian, M.** and **Rahnejat, H.** A dexterous anthropomorphic hand for robotic and prosthetic applications. *Robotica*, 1994, **2**.

3 **Medhian, M.** *A polymer sensor for monitoring of prosthetic vascular grafts.* Internal report, Robotics and Machine Intelligence Group, RMIG17, 1991.

4 **Montenson, J. D.** Safety and performance of currently available vascular prosthesis. *Trans. Am. Soc. Artif. Organs*, 1981, **4**(125).

APPENDIX 1

In the physical interpretation of functions ϕ and ψ it was shown above that these represent pressure wave functions. Furthermore, it was shown that $x_1 = \pm at + C_2$. Then

$$-v\frac{\partial v}{\partial x_1} = \pm\frac{v}{a}\frac{\partial v}{\partial t} \tag{17}$$

and

$$-v\frac{\partial H}{\partial x_1} = \pm\frac{v}{a}\frac{\partial H}{\partial t} \tag{18}$$

Since in a conduit the ratio of v/a is usually of the order of 1/100 or less, the terms $v(\partial v/\partial x_1)$ and $v(\partial H/\partial t)$ are negligible when compared with the terms $\partial v/\partial t$ and $\partial H/\partial t$ respectively.

APPENDIX 2

Solution to the pair of equations (12) and (13) is of the form stated by equations (14) and (15). To obtain the exact form the following procedure is undertaken:

Step 1 Partial differential of equation (12) with respect to time is obtained.
Step 2 Partial differential of equation (13) with respect to x_1 is obtained.
Step 3 The resulting partial differentials are one and the same (that is $\partial H/\partial x_1\,\partial t$), thus the results of steps 1 and 2 can be equated to yield the wave equation as

$$\frac{\partial^2 v}{\partial x_1^2} = \frac{1}{a^2}\frac{\partial^2 v}{\partial t^2} \tag{19}$$

The solution will be of the form $v = f(x, t)$.
Step 4 Considering any given prosthesis in a vascular graft, typical boundary conditions of the following form can be employed:

1. Fixed at both ends, thus $v(0, t) = v(L, t) = 0$ for $t \geqslant 0$.
2. The initial velocity at a point P at $t = 0$ is $v(x_p, 0) = f(x_p)$.
3. The initial rate of change of flow velocity at a point P at $t = 0$ is $(\partial v/\partial t)_{t=0} = g(x_p)$.

Step 5 Assume a trial solution of the form: $v(x, t) = H(x)v(t)$. A solution of the wave equation can now be undertaken by variable separation. This will lead to the following transposed form of the wave equation:

$$\frac{1}{H}\frac{\partial^2 H}{\partial x^2} = -\frac{1}{a^2}\frac{1}{v}\frac{\partial^2 v}{\partial t^2} \tag{20}$$

For the two sides of the above equation to be equal for values of the separated variables then both expressions can be equated to the same constant k. The value of k can be altered but would not lead to an oscillatory solution for $k \geqslant 0$. For $k < 0$, let $k = -Q^2$ and the following relations are obtained:

$$\frac{\partial^2 H}{\partial x^2} + Q^2 H = 0$$

and

$$\frac{\partial^2 v}{\partial t^2} - a^2 Q^2 v = 0 \tag{21}$$

For a solution of the form $V = Hv$, the following is obtained:

$$v_j(x, t) = \left[\left(A_j \cos\frac{\lambda x}{a} + B_j \sin\frac{\lambda x}{a}\right) \times (C_j \cos \lambda t + D_j \sin \lambda t)\right] \tag{22}$$

where

$$Q = \lambda/a.$$

Step 6 Implement the boundary conditions stated above at $x = 0$ and $x = L$. This leads to $A_j = 0$, and $B_j \sin(\lambda L/a)\{C_j \cos \lambda t - D_j \sin \lambda t) = 0$, where $B_j \neq 0$ and $\sin \lambda L/a = 0$ leads to an infinite set of λ values.

Eigenvalues:

$$\lambda = na\pi/L$$

Eigenfunctions:

$$v(x, t) = B \sin(\lambda x/a)\{C_n \cos \lambda t - D_n \sin \lambda t) \tag{23}$$

Step 7 Now for a general solution $v(x, t) = \sum_1^\infty v_j$ and using equation (23) above as v_j and Fourier series approximation, the equation (16) would result.